Journal of Nuclear Materials 403 (2010) 7–14

Contents lists available at ScienceDirect

Journal of Nuclear Materials

journal homepage: www.elsevier.com/locate/jnucmat

Micro-structural characterization of laboratory heats of the Ferric/Martensitic steels HT-9 and T91

P. Hosemann [a,b,*], S. Kabra [a], E. Stergar [b,c], M.J. Cappillo [a], S.A. Maloy [a]

[a] Los Alamos National Laboratory, MST-8, P.O. Box 1663, 87545 Los Alamos, NM, USA
[b] University of California, Department of Nuclear Engineering, Berkeley, CA 94720, USA
[c] Montanuniversität Leoben, Franz Josef Strasse 18, 8700 Leoben, Austria

ARTICLE INFO

Article history:
Received 10 March 2009
Accepted 6 May 2010

ABSTRACT

Ferritic/Martensitic materials such as T91 (9Cr–1Mo) and HT-9 (12Cr–1Mo) are candidate materials for nuclear reactor fuel cladding. In order to ensure a full understanding of these materials microstructure in this study a comprehensive characterization of these alloys was conducted. A heat of HT-9 and T91 was produced and the micro-structural changes from the as cast state to the final heat treated sheet product were characterized. Metallography revealed an overall picture of the different microstructures while neutron diffraction performed during the materials heat treatment revealed insight about texture, thermal expansion and transition temperatures. 3D atom probe showed the exact overall composition and the local composition the carbides formed in the material.

Published by Elsevier B.V.

1. Introduction

The Ferric/Martensitic stainless steel alloys HT-9 (12Cr–1Mo) and T91 (9Cr–1Mo) have beneficial properties (e.g. swelling resistance, low corrosion, good thermal conductivity, low thermal expansion, etc.) for advanced fast reactor application. The crystalline body centered cubic (bcc/bct) structure coupled with a large amount of interphases (martensitic laths) gives these samples great resistance to irradiation-induced swelling [1–6]. In Klueh and Nelson [7] an extensive study summarizing many results from the literature was presented. In addition, HT-9 has relatively good corrosion properties for fast reactor environment such as lead bismuth eutectic [8]. With the perspective of a nuclear renaissance it was found important to report a study of the materials state during and after proper heat treatments. It was found that a study reporting the crystal structure over temperature and to prove that the resulting carbides are indeed $M_{23}C_6$ carbide being present at the grain boundary might be needed. Especially since this particular heat of HT-9 and T91 is used at Los Alamos at different ion beam studies [1,9]. In this work the materials processing starting from casting to the final sheet product of HT-9 and T91 was performed and the material was analyzed in order to establish a baseline for future manufacturers and to report the material used for further experiments. After casting, samples of each alloy were deformed (forging and rolling) and heat treated. After the deformation and heat treatment, metallographic analyses were performed on the samples. In addition, neutron diffraction was performed during the heat treatment to analyze the exact thermal expansion (changes in d-spacing) texture and phase fractions.

2. Experiment

2.1. Materials synthesis

Heats of HT-9 and T91 were produced using a vacuum furnace with the capacity of producing a heat of 25 kg at one time. The composition was monitored during production. The exact composition of the materials HT-9 and T91 was determined from chemical analysis shown in Table 1.

The as cast material was cut in 20 mm thick slice and further forged and rolled. The forging took place at 1000 °C. The samples were hit with a pressure of 3.4 MPa three times in one direction and once on their side for a 30% reduction at each hit. After forging, the material was hot rolled in air at 900 °C to a final thickness of 6.35 mm. Then, the materials were heat treated according to the literature suggestions [3] to a tempered martensitic condition. This consisted of normalization at 1050 °C for 1 h in argon followed by an air cool and then tempered at 760 °C in argon followed by another air cool.

2.2. Analysis

In the following section, each analytical step is described in detail.

* Corresponding author at: Los Alamos National Laboratory, MST-8, P.O. Box 1663, 87545 Los Alamos, NM, USA. Tel.: +1 505 629 9893; fax: +1 505 667 7443.
E-mail address: peterh@lanl.gov (P. Hosemann).

0022-3115/$ - see front matter Published by Elsevier B.V.
doi:10.1016/j.jnucmat.2010.05.005

2.2.1. Metallography and hardness measurements

In between each production step, optical microscopy was performed on the materials. After cutting the samples using a slow speed cutting saw, the sample was ground and polished using SiC paper with 1200 grit followed by polishing down to 1 μm diamond polishing as a last step. After polishing, the sample was

Table 1
Results of the chemical analysis on HT-9 and T91 (units are in wt.%).

	O	N	C	S	V	W	P	Co	Cu	Ti	Fe	Mn	Si	Cr	Mo	Ni	Al
HT-9	0.016	0.031	0.171	0.004	0.34	0.58	0.007	0.009	0.025	0.002	84	0.61	0.41	12.1	0.97	0.59	0.007
T91	0.012	0.008	0.082	0.002	0.28	0.02	0.006	0.007	0.022	0.003	88	0.52	0.31	9.2	0.97	0.45	0.006

Table 2
Vickers micro-hardness measurements on the samples investigated.

	Cast HT-9	Cast T91	Forged HT-9	Forged T91	Hot rolled HT-9	Hot rolled T91	Heat treated HT-9	Heat treated T91
HV	460	368	492	370	254	278	306	269
Grain size (μm)	3246	3075	883	622	NM	NM	NM	NM

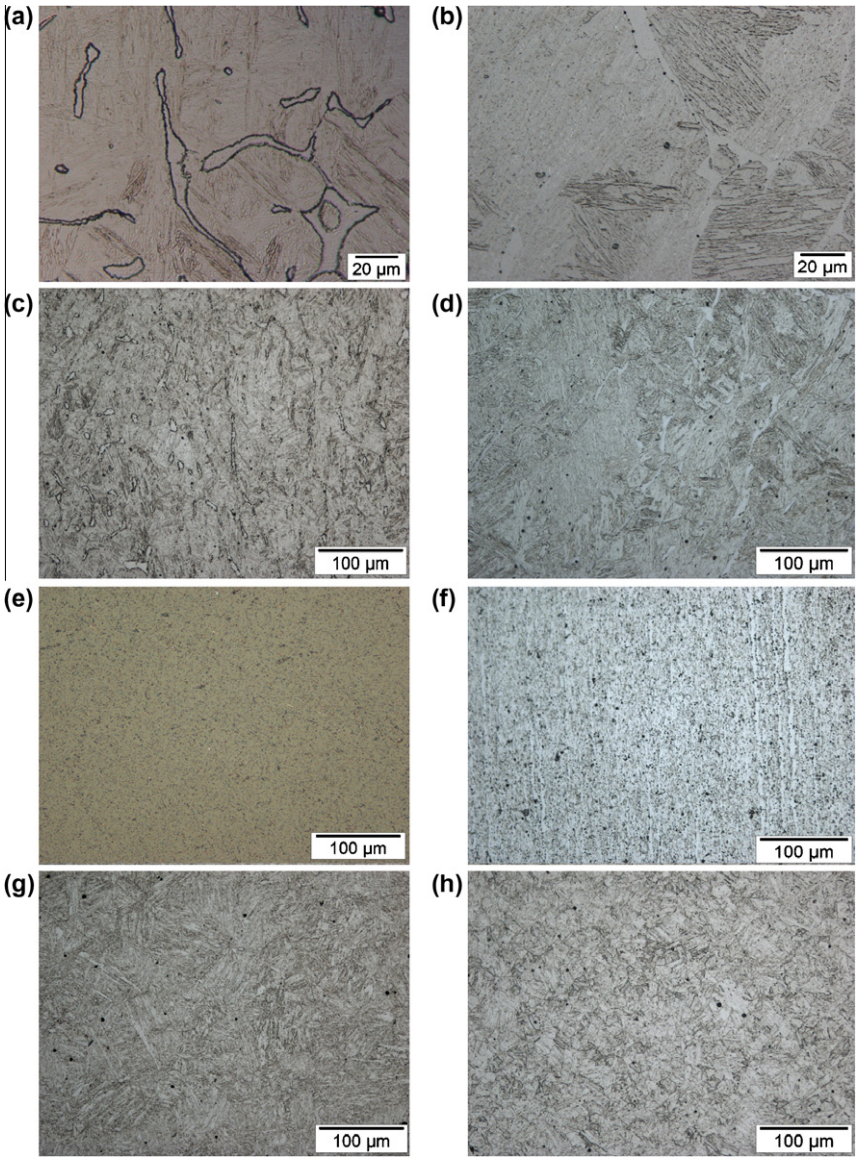

Fig. 1. HT-9 (a) and T91 (b) cast structure taken from equiaxed zone 500×. Micrograph from HT-9 (c) and T91 (d) of the forged material. Micrograph from HT-9 (e) and T91 (f) from the rolled materials. Micrographs from HT-9 (g) and T91 (h) from the fully heat treated material.

etched using an enchant acid mixture having the components 20 ml H_2O, 20 ml HNO_3, 20 ml HCl, and 10 ml HF.

Micro-hardness measurements were performed on each sample after polishing using a Buehler micromet-4 micro-hardness tester.

2.2.2. Neutron diffraction analysis

The phase changes during heat treatment were analyzed by performing neutron diffraction experiments using the High Pressure Preferred Orientation (HIPPO) instrument at Lujan center at Los Alamos National Laboratory. The furnace at HIPPO allows reaching a maximum temperature of 1050 °C while performing the neutron diffraction experiment. The samples were first heated to 1050 °C using a heating rate of 200 °C/h then furnace cooled and re heated to 760 °C (200 °C/h heating rate) followed by a furnace cooling step back to room temperature. In addition to determining the phase changes and phase fractions, HIPPO also allows for texture measurements during heat treatment. During the heating the sample was held for 5 min at a constant temperature so diffraction patterns with low background noise can be made. But in order to keep a fast cooling rate a diffraction pattern were taken every 2 min without holding the temperatures. Therefore the cooling patterns are much noisier and inaccurate since the data take is averaged over a temperature range of ~30 °C.

For important points in the temperature profile (at the beginning of the measurement at holding temperature, etc.) texture measurements were performed. During this measurement the sample was rotated to 0°, 45°, 67.5° and 90° to get full 360° sample coverage [10].

The post neutron diffraction data analysis was performed using the software GSAS [11].

2.2.3. 3D atom probe analysis

One sample of HT-9 as heat treated was analyzed using a Local Electrode Atom Probe (LEAP) system (LEAP 3000x-HR) located at the Montanuniversität Leoben in Austria. The measurements were performed under ultra high vacuum condition with a puls repetition rate of 200kHz at a temperature of 47 K. Several LEAP samples were measured while one with a large carbide is presented in Fig. 6. Ten million atoms were collected on the sample shown. The reconstruction and post measurement analysis was performed using the software IVAS™ (Imago Visualization and Analysis Software) from IMAGO INC. [12].

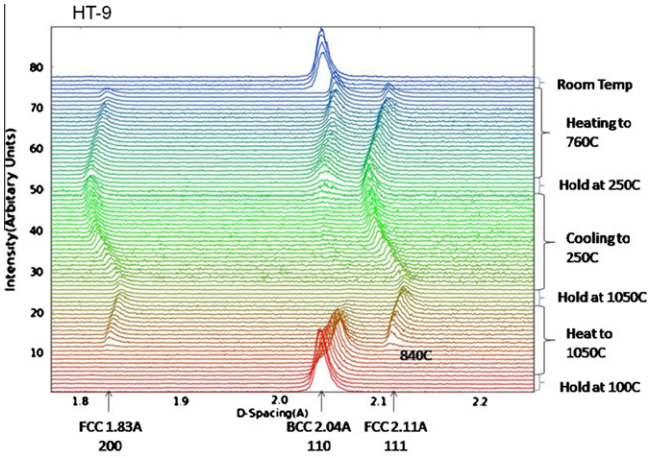

Fig. 2. T91 neutron diffraction data graph from HIPPO.

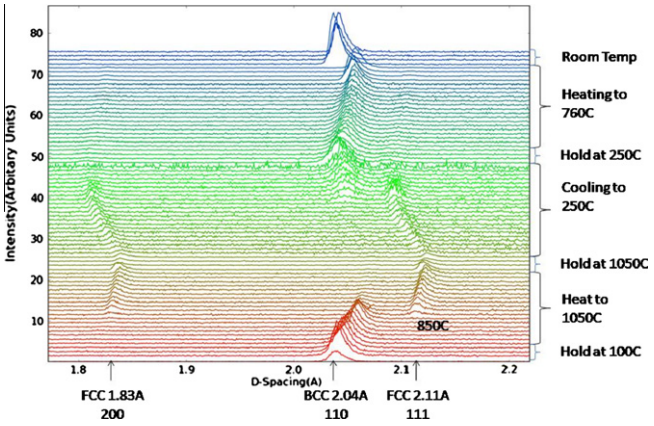

Fig. 3. Texture plots of the sample HT-9 at the beginning of the experiment (a) 1050 °C (b), after the cooling cycle at 760 °C for bcc (c) and fcc (d). HT-9 at 750 °C fcc (e), bcc (f) and 200 °C (g).

Table 3
Lattice constant calculated form the d-spacing measurements of the orientation [2 0 0] of the HIPPO experiment. Only the data of the first heating cycle are shown. All units are in nm. HT-9 was heated up to 1050 °C, T91 was heated up to 1060 °C.

Temperature (°C)	HT-9 bcc (nm)	Error (fm)	HT-9 fcc (nm)	Error (fm)	T91 bcc (nm)	Error (fm)	T91 fcc (nm)	Error (fm)
100	0.2881362	6.20	–	–	0.2878274	15	–	–
200	0.2884986	6.00	–	–	0.2885794	9.20	–	–
300	0.2887812	6.10	–	–	0.2887890	10.0	–	–
400	0.2890890	6.10	–	–	0.2891698	10.6	–	–
500	0.2894022	6.20	–	–	0.2895220	11.3	–	–
600	0.2897318	5.90	–	–	0.2898108	13.1	–	–
700	0.2900324	5.30	–	–	0.2901842	10.9	–	–
800	–	–	0.3649338	55.9	0.2906470	8.80	–	–
820	–	–	0.3650228	27.5	0.2907602	11.2	–	–
840	–	–	0.3652686	12.8	–	–	0.3652516	33.2E
860	–	–	0.3654266	92.0	–	–	0.3655102	14.1
880	–	–	0.3655506	96.0	–	–	0.3656996	13.6
900	–	–	0.3657624	11.3	–	–	0.3658752	14.0
920	–	–	0.3660032	10.1	–	–	0.3660614	11.8
940	–	–	0.3661674	10.2	–	–	0.3662132	11.8
960	–	–	0.3664386	99.0	–	–	0.3664354	14.0
980	–	–	0.3667162	10.4	–	–	0.3666182	13.1
1000	–	–	–	–	–	–	0.3667920	13.5
1020	–	–	–	–	–	–	0.3669198	14.1
1040	–	–	–	–	–	–	0.3671124	15.5
1050/1060	–	–	0.3675838	7.90	–	–	0.3666414	7.6

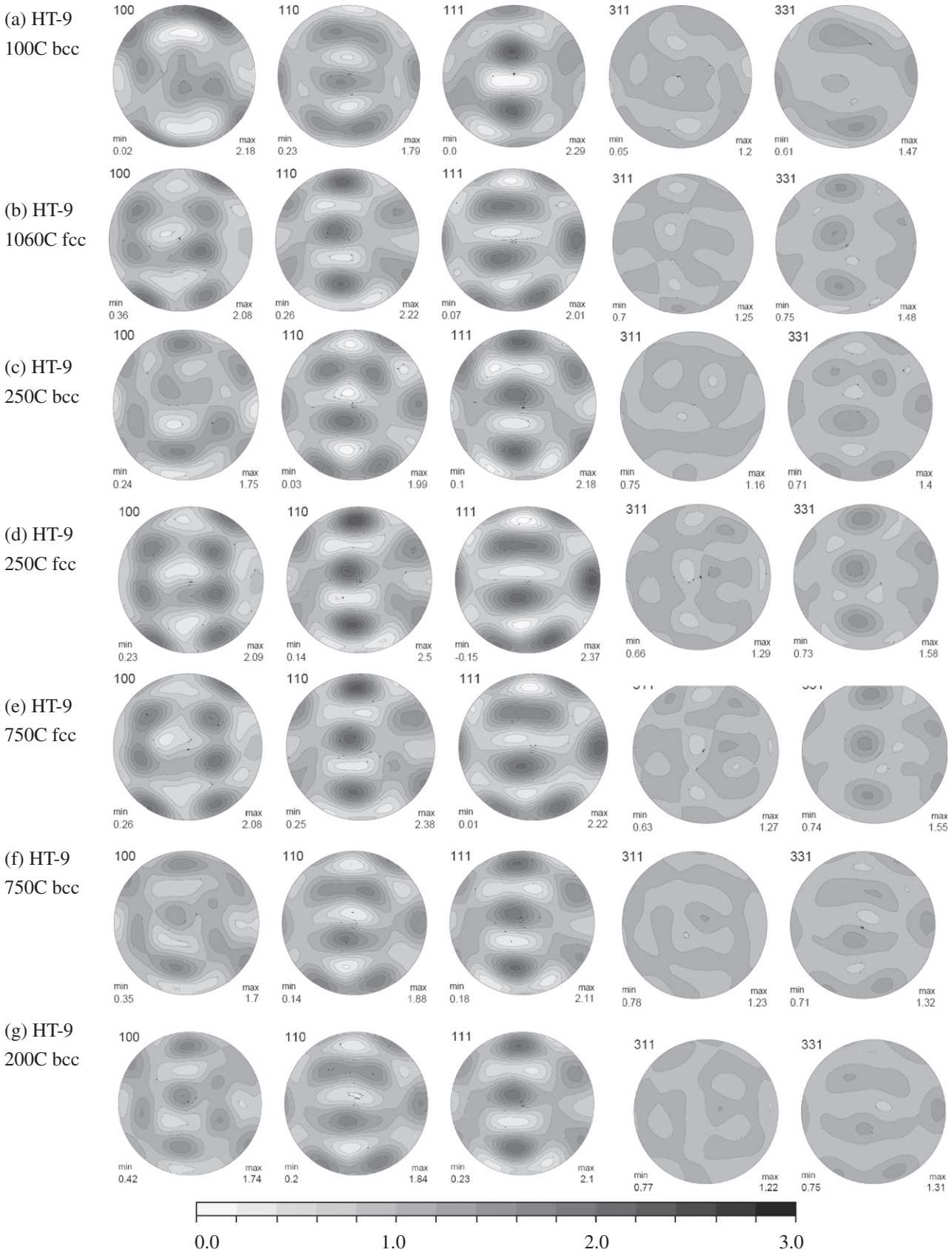

Fig. 4. Texture plots of the sample T91 at the beginning of the experiment (a) 1050 °C (b), after the cooling cycle at 250 °C (c) at 760 °C (d) and at 175 °C (e).

3. Results

3.1. Metallography and micro-hardness results

Metallographic analysis and micro-hardness measurements were performed on all the samples. The results of the micro-hardness measurements can be seen in Table 2. After casting a course Perlite/Ferrite structure it can be seen in Fig. 1. After forging the large grained structure is disrupted. The hot rolling causes a slight texture in the material. After the full heat treatment a fine Ferritic lath structure is observed. The fine structured material makes it difficult to measure an accurate grain size therefore this was not measured.

T91 seem to have less of a martensitic lath structure than HT-9. The micro-hardness shows that T91 is significant softer than the HT-9.

3.2. Neutron diffraction

The results of the HIPPO measurements and GSAS peak fits performed on HT-9 and T91 after the hot rolling stage are presented in Table 3 and Figs. 2–5. In Figs. 2 and 3 the d-spacing are plotted vs.

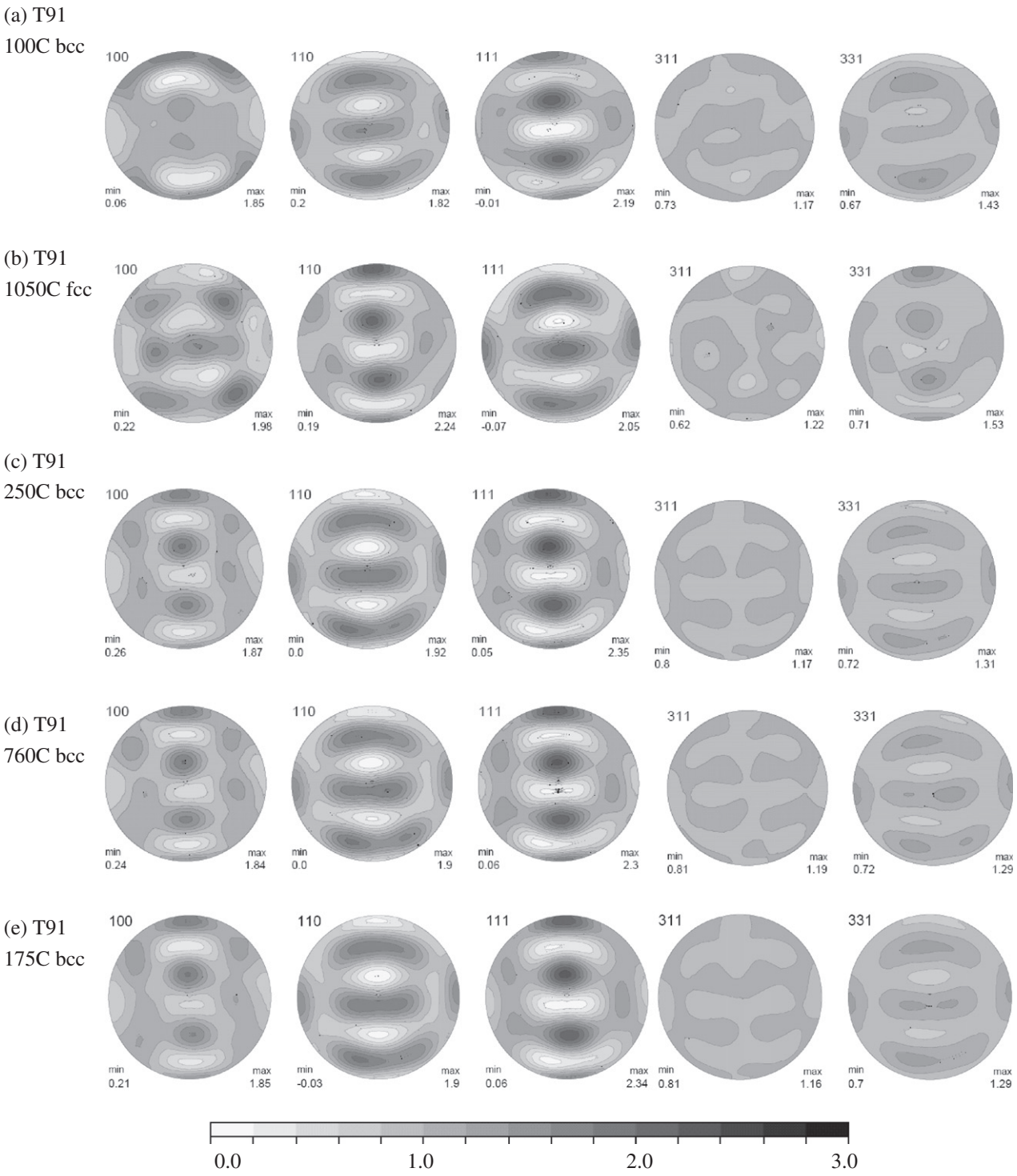

Fig. 5. LEAP results on HT-9 (a) and line scan across the carbide found in the tip (b). EELS TEM images of HT-9 (c) and (d).

intensity for all the measurements taken at different temperatures. These plots show the phase transformations at the temperature and the thermal expansion. It appears that the HT-9 material transforms to Austenite at around 840 °C and stays austenitic also during the furnace cooling. Only the tempering at 760 °C allows the material to transform into bcc. Following the quenching from tempering 49.3 vol.% of the material is still fcc and 50.7 vol.% is bcc. During annealing the volume fraction of bcc increases up to 69.3 vol.% while the fcc phase fraction reduces to 30.7 vol.% at 760 °C in HT-9. At the end of the slow cooling cycle the material is fully bcc. The texture plots taken at each significant temperature (100 °C, 1060 °C, 250 °C, 750 °C) and room temperature are given in Fig. 4. It can be seen that there is a slight texture (1 1 1) in rolling direction. This slight texture seem to be present throughout the entire heat treatment cycle.

The material T91 seem to transform into austenite at 850 °C and transforms back into bcc at the quenching step at a temperature around 300 °C. At the end of the heat treatment cycle (room temperature) it can be seen that the material is fully bcc after the quenching and before the actual annealing step. It is clear that the material transforms easier into bcc than the HT-9 does. The texture plots taken at the holding temperatures are shown in Fig. 5. It can be sent hat the material has a 2.2 times random structure of (1 1 1) in the rolling direction as well. No obvious difference between HT-9 and T91 can be seen.

3.3. 3D atom probe and TEM results

The 3D atom probe results are presented in Fig. 6b and c. In this particular measurement carbides were found. It can be clearly seen that the carbide is enriched in Cr, C, and slightly V and W. Fe and Si is depleted. The line scan shows more detail (Fig. 6c). The TEM-EELS data indicate that the carbides are mainly found on grain boundaries and that the grain structure is rather fine 2–5 μm (Fig. 6d and e).

4. Discussion

In all treatment stages some carbide are visible. It appears that after the heat treatment these carbides are located at the grain boundaries mainly (Fig. 6). The LEAP measurements clearly show that the carbides consist of 50 at.%Cr, 20 at.%C, 25 at.%Fe and others (W, V, Si) which can be related to $M_{23}C_6$ with mainly Cr as the metal. No significant Cr depletion or Fe enrichment was found surrounding the carbide. The TEM shows that the carbides are mainly located at interfaces. This is in agreement with a study conducted on X20CrMoV12.1 [13].

Considering that this heat of HT-9 has 2 times the amount of C than T91 the difference in hardness should be related to this fact. In this study no chromium depletion was found but ~0.08 wt.% more C (in HT-9 than in T91) are able to bind about 1.4 wt.% of additional Cr in $M_{23}C_6$ carbides. Since HT-9 has 3 wt.% more Cr it is assumed that a local depletion around carbides is supplied by the 3 wt.% more Cr in the material preventing corrosion phenomena.

The excessive hardness of the HT-9 and T91 after casting is based on the cementite present in this microstructure. While forging only refines the microstructure the material increase its hardness slightly. Only the rolling and heat treatment at higher temperature allows getting a fine structured Ferritic microstructure. This shows

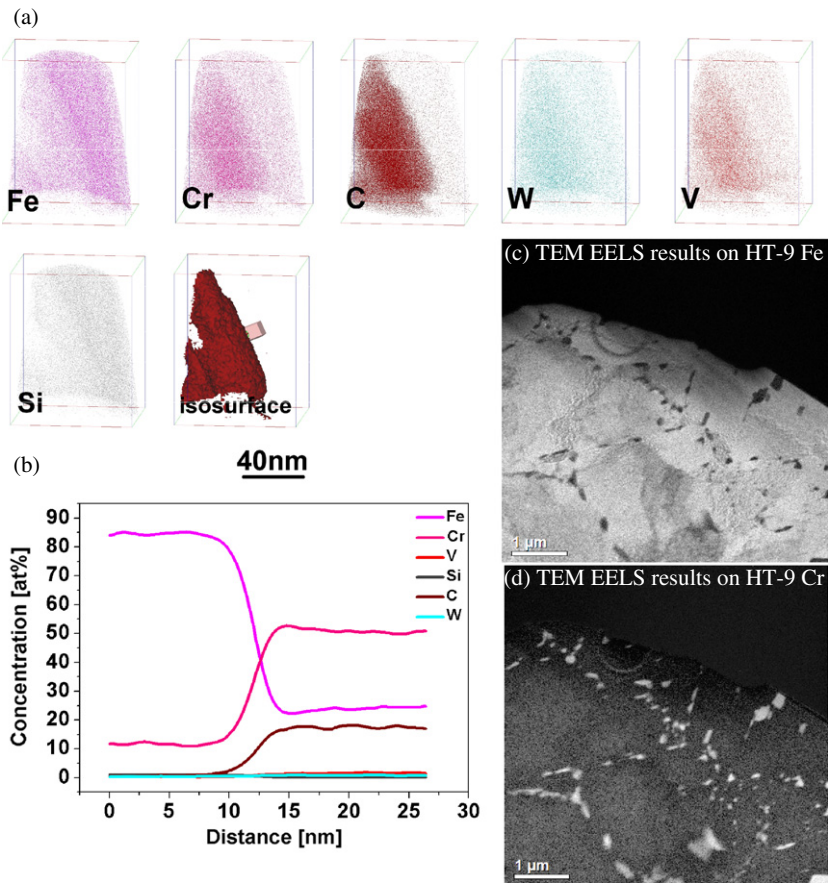

Fig. 6. Plots of the thermal lattice expansion on HT-9 (a) and T91 (b).

clearly that a reactor component needs to undergo a full heat treatment before it can be used as component.

The HIPPO analysis shows clearly that with the range of austenitization both materials have a bcc to fcc phase change at around 850 °C. This agrees temperature range of TTT diagrams for X20CrMoV12 where the AC2 temperature is 870 °C [14]. During cooling it seems that T91 transforms back to bcc at about 300 °C while the HT-9 does not transform back to bcc during the first cooling cycle. Only the tempering after quenching allows the HT-9 to transform to bcc. It appears that the higher alloying composition of HT-9 requires a higher driving force for the material to change its phase. But since HIPPO does not allow higher cooling rates HT-9 cannot transform at this given cooling rates. Only the annealing steps allow the full bcc transformation to happen.

Using the C equivalent equitation given in [15] it can be found that the Ms temperature for HT-9 is 276 °C and the Mf temperature is 61 °C while T91 has a Ms temperature of 350 °C and Mf 134 °C. This temperatures are similar to what can be found in the TTT diagram of [14] for X20CrMoV12 where at a temperature of 200 °C and a cooling rate of 800 °C/1000 s a Ms volume fraction of ~50% can be seen. This agrees with the values found here and explains while the material HT-9 did not fully transform into martensitic after the first quenching step while the material T91 did.

In addition to the phase identification the peak shift with temperature can be used to determine the thermal expansion of the lattice. Fig. 7 presents the lattice expansion vs. temperature for the bcc and fcc phase on HT-9 and T91.

Table 3 presents the actual measured lattice spacing and d-spacing measured. Comparing the material T91 and HT-9 no significant difference in the lattice expansion was found. Both materials have a larger lattice constant than what is reported in the literature [16,17] for pure Fe. This is also in agreement with the literature where Fe–Cr alloys were reported to have a lattice constant at room temperature for Fe:Cr = 1:1 of 2.900 Å [18]. For HT-9 a thermal expansion of the bcc phase of 3.33×10^{-5} Å/°C and a lattice expansion of 1.06×10^{-4} Å/°C was found. While T91 shows a thermal expansion of the bcc phase of 4.07×10^{-5} Å/°C and a lattice expansion of 6.6×10^{-5} Å/°C.

A lattice expansion of 3.33×10^{-5} Å/°C would lead to thermal expansion of 11.6 μm/mK. It is known that 420 stainless steel (a similar 13%Cr steel) has a thermal expansion of 12.1 μm/mK in the temperature range of 0–649 °C. Considering the uncertainty the measurements performed here are clearly within the correct range.

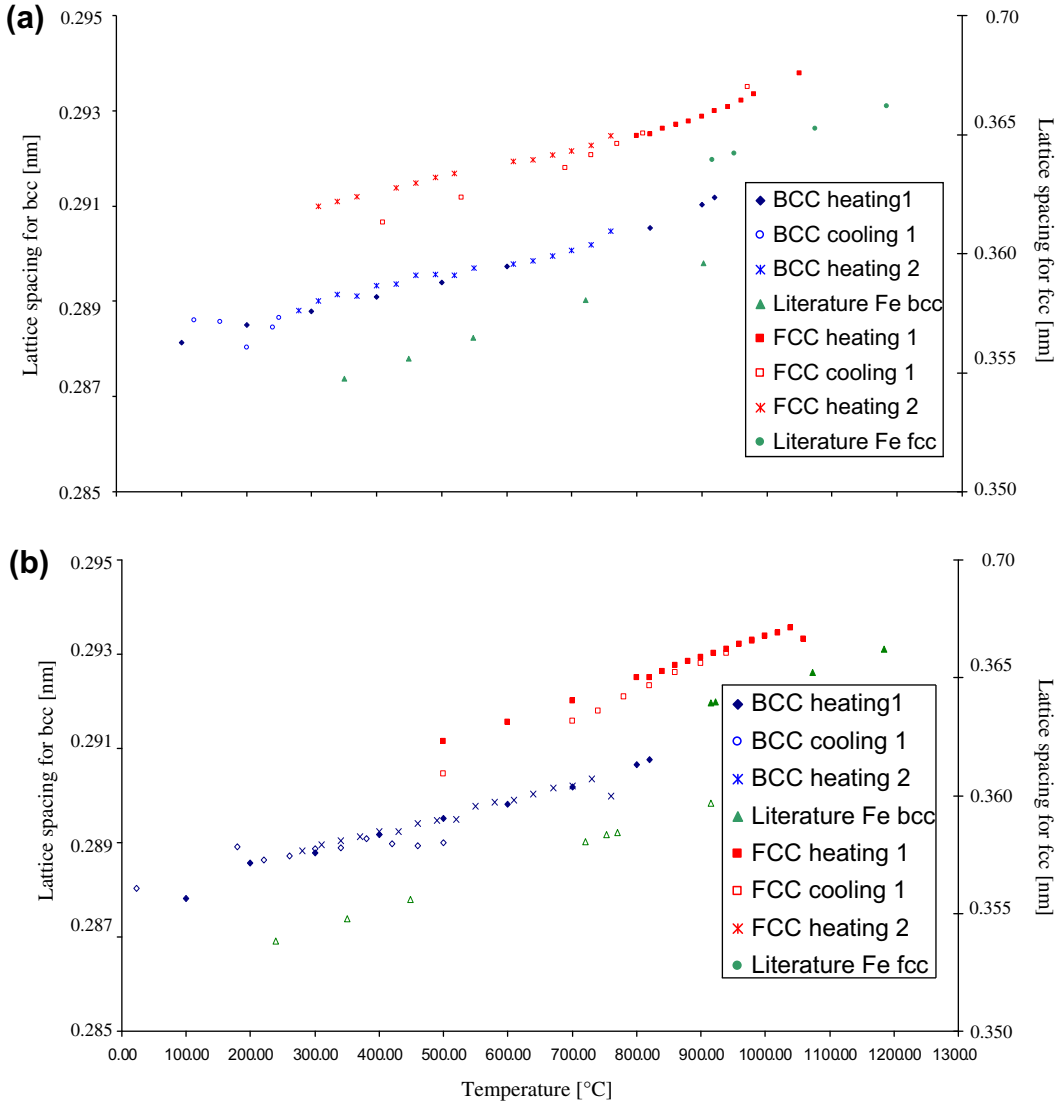

Fig. 7. Plots of the thermal lattice expansion on HT-9 (a) and T91 (b).

No other phase than the Fe–Cr bcc and fcc phase were found at this experiment. But phase fractions below 2–5% cannot easily be detected using HIPPO.

The texture analysis shows that neither material does show a strong texture at any state of heat treatment (Figs. 4 and 5).

5. Summary

- The materials HT-9 and T91 were produced and tested. The production procedure and results match the data from the literature for HT-9 and T91.
- The 3D atom probe and TEM measurements confirmed that the particles found at the grain boundary are $M_{23}C_6$ carbides with mainly Cr as the metal. The carbides are located mainly at the grain boundaries.
- The neutron diffraction measurements allowed measuring accurately the increase of lattice spacing with temperature as well as the phase transformation temperature. The lattice constant increase with temperature agrees very well with the literature values and the macroscopic thermal expansion coefficients given in similar materials datasheets. This result can be used as a base for engineering application at elevated temperatures.
- HIPPO allows also to measure texture on the samples. It was found that the rolling texture is removed after the heat treatment to the martensitic state. No difference in texture was found.

Acknowledgements

The authors want to thank G. Jesner for supplying TTT diagram information, M.J. Cappiello for assisting by preparing the metallographic specimen and R. Dickerson for supporting the TEM data analysis.

This work has benefited from the use of the Lujan Neutron Scattering Center at LANSCE, which is funded by the Office of Basic Energy Sciences (DOE). Los Alamos National Laboratory is operated by Los Alamos National Security LLC under DOE Contract DE-AC52-06NA25396.

References

[1] P. Hosemann, C. Vieh, R.R. Greco, S. Kabra, J.A. Valdez, M.J. Cappiello, S.A. Maloy, J. Nucl. Mater. 389 (2009) 239–247.
[2] P. Hosemann, J.G. Swadener, D. Kiener, G.S. Was, S.A. Maloy, N. Li, J. Nucl. Mater. 375 (2008) 135–143.
[3] M.B. Toloczko, F.A. Garner, J. Nucl. Mater. 233 (1996) 289–292.
[4] M.B. Toloczko, F.A. Garner, C.R. Eiholzer, J. Nucl. Mater. 212 (1994) 604–607.
[5] S. Yamashita, Y. Yano, Y. Tachi, N. Akasaka, J. Nucl. Mater. 386–388 (2009) 135–139.
[6] M. Matijasevic, E. Lucon, A. Almazouzi, J. Nucl. Mater. 377 (2008) 101–108.
[7] R.L. Klueh, A.T. Nelson, J. Nucl. Mater. 371 (2007) 37–52.
[8] P. Hosemann, M.E. Hawley, D. Koury, J. Welch, A.L. Johnson, G. Mori, N. Li, S.A. Maloy, J. Nucl. Mater. 381 (2008) 211–215.
[9] D.C. Foley, K.T. Hartwig, S.A. Maloy, P. Hosemann, X. Zhang, J. Nucl. Mater. 389 (2009) 221–224.
[10] S.C. Vogel, C. Hartig, L. Lutterotti, R.B. Von Dreele, H.R. Wenk, D.J. Williams, Adv. X-ray Anal. 47 (2003) 431–436.
[11] A.C. Larson, R.B. Von Dreele, GSAS Software.
[12] IVAS™ Software Package IMAGO INC.
[13] D.A. Skobir, M. Godec, M. Jenko, B. Markoli, Surf. Interf. Anal. 40 (2008) 513–517.
[14] Boehler Steel Data Sheet on X20CrMoV12, Boehler Austria.
[15] Handbuch der Böhler Schweißtechnik Austria GmbH, Ausgabe 09/2006.
[16] H.E. Swanson, E. Tatge, Adv. X-ray Anal. 5 (1961) 57–63.
[17] Z.S. Basinski, W. Hume-Rothery, A.L. Sutton, Proc. R. Soc. London Ser. A229 (1955) 459.
[18] T.I. Badjuk, G.P. Kushma, O.I. Rybajlo, Metallofizkika 41 (1972) 73–77.